ACS APPLIED NANO MATERIALS

www.acsanm.org

Article

DNA-Based Optical Sensors for Forces in Cytoskeletal Networks

Christina Jayachandran,[¶] Arindam Ghosh,[¶] Meenakshi Prabhune, Jonathan Bath, Andrew J. Turberfield, Lara Hauke, Jörg Enderlein, Florian Rehfeldt,* and Christoph F. Schmidt*

Cite This: *ACS Appl. Nano Mater.* 2023, 6, 15455−15464

Read Online

ACCESS | Metrics & More | Article Recommendations | Supporting Information

ABSTRACT: Mechanical forces are relevant for many biological processes, from wound healing and tumor formation to cell migration and differentiation. Cytoskeletal actin is largely responsible for responding to forces and transmitting them in cells, while also maintaining cell shape and integrity. Here, we describe a FRET-based hybrid DNA-protein tension sensor that is designed to sample transient forces in actin networks by employing two actin-binding motifs with a fast off-rate attached to a central DNA hairpin loop. Such a sensor will be useful to monitor rapidly changing stresses in the cell cytoskeleton. We use fluorescence lifetime imaging to determine the FRET efficiency and thereby the conformational state of the sensor, which makes the measurement robust against intensity variations. We demonstrate the applicability of the sensor by confocal microscopy and by monitoring crosslinking activity in *in vitro* actin networks by bulk rheology.

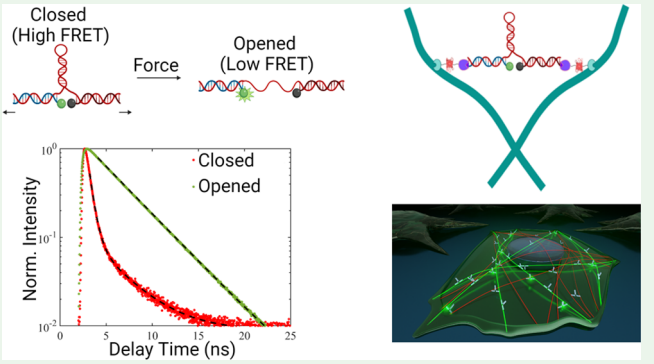

KEYWORDS: *molecular force sensors, fluorescence lifetime imaging microscopy, cytoskeleton, actin, DNA, stress fibers*

INTRODUCTION

The actin cytoskeleton,[1] interacting with myosin motors, is the dominant force-generating machinery in most cells. For example, stress fibers[2] produce contractile forces,[3,4] which help in cell locomotion, division,[5] and differentiation.[6] Propulsive forces of ca. 20 pN that are generated by actin polymerization[7] drive cell migration.[8−10] In conjunction with myosin motors, actin also serves as a key element in mechanosensation.[11,12] Force-transmitting and sensing structures as well as their movements can readily be imaged in fluorescence microscopy. For example, on rigid substrates, cells form prominent actin stress fibers.[13−15] While strains can be readily imaged, forces and stresses are not directly visible, and it remains challenging to quantitate forces on actin structures in cells due to the lack of appropriate force sensors.

Several methods have been applied to measure cellular forces transmitted to their surroundings, including traction force microscopy,[16] atomic force microscopy,[17,18] and optical[19,20] and magnetic tweezers.[21] However, these methods are insensitive to internally balanced forces in the cells and thus cannot sample intracellular stresses. It is important to realize, in any case, that molecular force sensors will never be able to completely map intracellular stresses since the sensor can only report on the force it transmits itself, while other cellular structures likely bear and transmit forces in parallel. Such sensors are thus best suited to qualitatively monitor rapidly changing stresses in dynamic regions of the cell cytoskeleton. The sensor design we introduce here achieves sensitivity to changes in stresses and rapid sampling of different binding geometries in the cytoskeletal networks to which it is attached by using an actin-binding motif with a reasonably high off-rate. This design effectively provides a high-pass filter function, which makes the sensor sensitive to rapid changes, but prevents it from getting stuck in a statically loaded or unloaded configuration. The off-rate of the binding motifs sets the high-pass filter frequency which can be modified by choosing different binding moieties (different ABPs) or by duplicating binding moieties. Other recent additions to the set of available tension-sensing methods are genetically expressed molecular force sensors (MFS) that rely on Förster resonance energy transfer (FRET). FRET-based MFS allow one to sample stresses by measuring the energy transfer efficiency between a donor and an acceptor fluorophore (FRET pair) that are coupled via a molecular spring.[22] These MFS offer pico-Newton (pN) sensitivity and high spatial (∼20 nm) and temporal resolution (∼ms) while minimally perturbing the cells.[23] However, genetically expressed sensors typically use fluorescent proteins[24,25] that can unfold upon force application and that possess photophysical properties inferior to those of organic dyes. When using polymer chains as molecular springs

Received: May 8, 2023
Accepted: June 16, 2023
Published: August 18, 2023

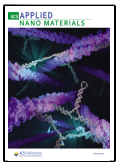

between donor and acceptor,[26,27] it is difficult to precisely adjust the spring stiffness. Both these limitations can be overcome by DNA-based MFS, which can be adjusted to a broad range of physiologically relevant forces[28] due to the easy designability of DNA structures[29−31] as referenced in Prabhune *et al.*[32] DNA-based MFS grafted on surfaces have been used to investigate interfacial forces between cells and ligands.[30,31]

The design of the tension sensor we present here uses a DNA hairpin that can switch between two conformational states,[33,34] and a FRET pair consisting of an organic dye (donor) and a quencher (acceptor) (Figure 1). This sensor

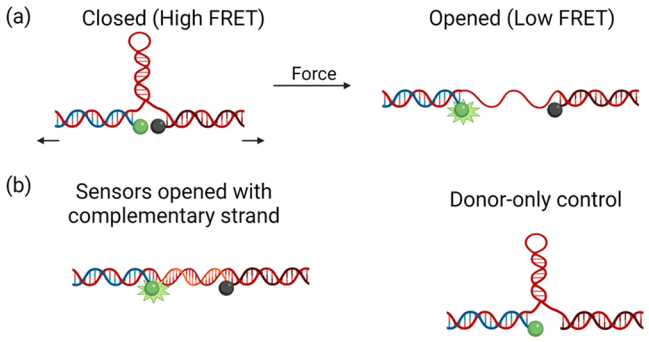

Figure 1. Design and attachment strategy of the DNA force sensor. (a) The DNA force sensor consists of a hairpin (red) with stem (8 bp), loop (16 bp), and two arms (each 20 nt). The arms hybridize with two strands, each 20 nt long, bearing the fluorophore Alexa 488 (F strand, blue) and quencher Iowa black FQ (Q strand, black) which form the FRET pair. A threshold force applied to the ends of the sensor opens it, switching it from its quenched state (high FRET) to its fluorescent state (low FRET). (b) For characterization purposes, sensor hairpins were opened using a complementary strand (orange). A donor-only control was designed lacking the quencher.

provides fluorescence read-out through a change in FRET efficiency when an external force pulls the hairpin apart. Actin-binding motifs are attached to the two ends of the DNA strand using the HaloTag system. The hairpin switches reversibly between two states: it opens at a specific threshold force and folds back when the force is lifted. The threshold opening force of DNA sensors similar to ours has been estimated to be ∼10 pN.[35,36] We estimated the threshold force for our sensors, i.e., the force $F_{1/2}$ at which 50% of our sensors would be expected to be open, based on free energy differences and geometrical parameters for both *in vitro* and *in cellulo* ionic conditions and temperatures. *In vitro* we find $F_{1/2} \approx 12$ pN and in a typical cell $F_{1/2} \approx 6$ pN (see the Supporting Information (SI) for calculations). In the following sections, we present the design and fabrication of this sensor, thoroughly characterize it by fluorescence lifetime imaging and spectroscopy, explore novel attachment strategies, check its performance in reconstituted actin networks, and report on a pilot study demonstrating that the sensors can be inserted into and targeted to the actin cytoskeleton in living cells.

EXPERIMENTAL SECTION

Sensor Sequence Design and Chemical Modifications. Sensor sequences (see Table S1) were designed on the NUPACK website,[37] and DNA oligomers were purchased from Integrated DNA Technologies (Leuven, Belgium). Lyophilized powders were reconstituted to 100 or 500 μM stock concentrations by adding an appropriate volume of DNA hybridization buffer (see Table S2). Sensors were further chemically modified at the 3′ end of the F strand and the 5′ end of the Q strand (see Table S1). These strands were purchased with thiol groups incorporated at the respective ends (see Table S1). Both strands were separately modified. Between 50 and 100 μL of 30 μM solutions of these strands were prepared by dilution in DNA hybridization buffers and reduced with 2 mM TCEP (Tris(2-Carboxyethyl)phosphine hydrochloride, Sigma-Aldrich, Germany) by incubating at room temperature for 60 min. Next, iodoacetamide (O_4) HaloTag ligand (Promega, Germany) was added to the above solution to a final concentration of 20 μM and incubated for 90 min.

Assembly of DNA Sensors. A volume of 50 μL of a solution of closed sensors or donor-only controls was prepared by adding chemically modified F strand (to 5 μM), Q or Q^- strand (to 10 μM), and a nonmodified H strand (to 10 μM final concentration) to DNA buffer. Opened sensors were assembled in the same way, followed by the addition of the C strand (complementary strand to hairpin loop). The molar concentration of the C strand was 10 times higher than that of the H strand. The final concentrations of sensors and donor-only controls were varied depending on the experiment (see Table

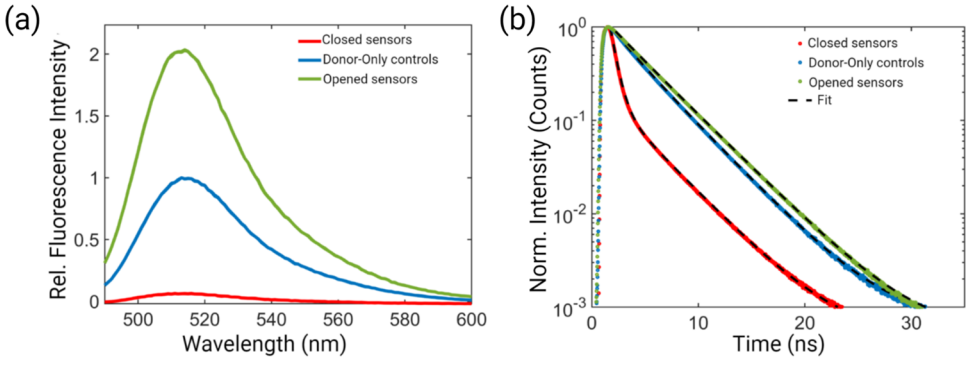

Figure 2. (a) Bulk fluorescence intensity measurements of DNA sensors. Experiments were performed with a commercial spectrometer recording emission spectra at an excitation wavelength of 488 nm. Spectra were normalized to the peak intensity of donor-only (blue) controls. Closed sensors in a DNA buffer exhibit a fluorescence signal (red) which is 90 ± 2% quenched compared to donor-only controls (blue curve). Additionally, the fluorescence intensity of opened sensors (green) is shown. Solid lines represent the mean value of fluorescence intensity from three consecutive measurements. (b) Fluorescence lifetime measurements of sensor molecules in aqueous buffer. Representative normalized TCSPC histograms and fits for closed sensors (red), donor-only controls (blue), and opened (green) sensors, respectively. Strong quenching of fluorescence in closed sensors (red) is visible corroborating the findings presented in (a). Opened sensors (green) exhibit a longer fluorescence decay compared to donor-only controls (blue) confirming the removal of intra-loop guanosine quenching upon hybridization and opening up of sensors.

https://doi.org/10.1021/acsanm.3c01783
ACS Appl. Nano Mater. 2023, 6, 15455−15464

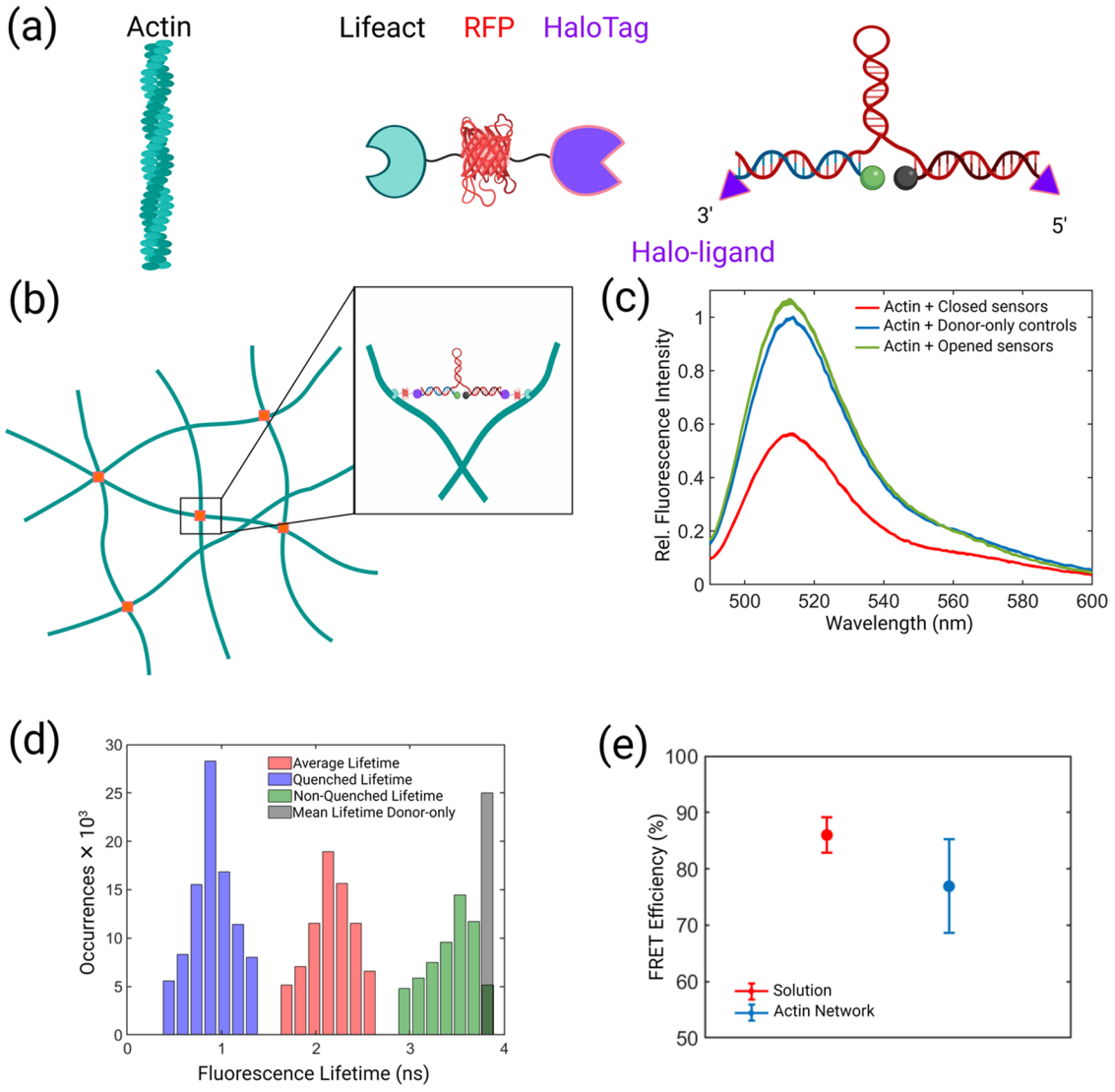

Figure 3. Fluorescence lifetime imaging microscopy (FLIM) of *in vitro* actin networks crosslinked by DNA sensors. (a) Attachment strategy for crosslinking the DNA sensors to *in vitro* reconstituted actin networks (molar ratio $R = 0.1$, $R = c_{crosslinker}/c_{actin}$). Extreme right: The outer ends of the F and Q strands are modified with a HaloTag ligand. The HaloTag ligands bind covalently to HaloTags via HaloTag fusion.[43] HaloTags were genetically expressed in *E. coli* cells, as a fusion with RFP and LifeAct, an actin-binding peptide[42] and produced as a protein that attaches to HaloTag-ligand-modified sensor molecules. (b) Schematic of DNA-sensor crosslinked actin network. The zoomed view shows the attachment of sensor molecules to the actin filaments. (c) When attached to an actin network ($R = 0.1$), the fluorescence intensity of closed sensors (red) is quenched; however, the quenching is much weaker (~50%) compared to sensors in solution 2a. (d) Fluorescence lifetime distributions for sensors attached to actin networks. Bar plots represent quenched lifetimes (blue) (0.8 ± 0.3 ns), nonquenched lifetimes mainly originating from quencher molecules and sensors lacking proper assembly (green) (3.4 ± 0.3 ns), and their intensity-weighted average lifetime (red) (2.1 ± 0.4 ns). The mean fluorescence lifetime of donor-only controls (3.8 ns) is shown in gray. Corresponding TCSPC decays and lifetime fits are presented in Figure S5. (e) FRET efficiencies of sensors in solution (red) and in *in vitro* actin networks (blue) were calculated to be 86 ± 3.2 and 77 ± 8.3%, respectively.

S3), while the ratios were kept constant at 0.5:1:1 (F/H/Q) in all experiments.

Actin and Actin-DNA Sensor Network Preparation. G-actin was prepared from rabbit skeletal muscle according to published protocols.[38−40] Purified actin was stored in small aliquots at −80 °C. Aliquots were thawed freshly prior to experiments. Concentrated 10× polymerization buffer (for actin buffer composition see Table S2, Polymix 10×, Hypermol) was added to an appropriate volume of water. G-actin was added to reach a final concentration of 24 μM (1 mg/mL). The concentration of actin remained unchanged throughout the experiments. To construct actin-DNA sensor networks, Lifeact-RFP-HaloTag protein was added to a final concentration of 30 μM. Then, modified and assembled sensors or donor-only controls, prepared as described above, were added. The sensor concentrations were varied from 0 to 4.7 μM (molar ratio R, see Table S3). For imaging experiments, a 10% volume from a 10 nM stock solution of Atto 647N, phalloidin (Atto-TEC GmbH, Siegen) was finally added. The solutions were gently pipetted to mix components and then filled into a microscope chamber (as described in the Confocal Imaging of Networks section).

The LifeAct-RFP-HaloTag proteins used to attach the sensors to *in vitro* actin networks were bacterially expressed, purified following standard procedures (see the SI) and added to the above-described chemically modified F and Q strand solutions. The LifeAct-RFP-HaloTag covalently binds to the iodoacetamide (O_4) HaloTag ligand on the F and Q strands.

Fluorescence Intensity Measurements. Fluorescence intensity measurements were performed with an AMINCO-Bowman Series 2 Luminescence Spectrometer (Thermo Electron Scientific Instruments Corporation, Madison, WI 53711). Emission spectra were measured

https://doi.org/10.1021/acsanm.3c01783
ACS Appl. Nano Mater. 2023, 6, 15455−15464

with the following instrument settings: Excitation wavelength—488 nm, emission wavelength—520 nm, bandpass—1, emission scan range 490−600 nm. For fluorescence intensity measurements of sensors & donor-only controls in solution (Figure 2, without lifeact-RFP-HaloTag), the closed sensors (FHQ), opened sensors (FHQC) and donor-only controls (FHQ-) were directly assembled in DNA buffer to the desired final volume. The outer ends of F and Q strands in these constructs were not functionalized with Lifeact-RFP-HaloTag and thus retained their thiol groups as obtained commercially. For fluorescence intensity measurements of the actin-DNA sensor network with R = 0.1 (Figure 3), the F and Q strands were first chemically modified to incorporate iodoacetamide (O_4) HaloTag ligands and then assembled as described in the Assembly of DNA Sensors section. Sensors were added to actin as described in the Actin and Actin-DNA Sensor Network Preparation section, pipetted into a cuvette, and placed inside the spectrometer. Emission scans were recorded after an hour of network polymerization at room temperature.

Rheology Measurements. Rheology measurements were performed with a commercial rheometer (MCR 501 Anton Paar, Austria) in a cone-plate geometry (CP-25, 2°). Polymerization of networks was monitored in time-sweep measurements with an oscillatory shear at 1% strain amplitude, 1 Hz frequency, at a temperature of 23 °C. To prevent evaporation during the measurements, sample hydration was maintained by placing wet tissue paper around the measurement plates. Frequency-dependent viscoelastic properties of the network were determined from frequency-sweep measurements, performed after the time sweeps for all networks. The frequency range was 0.01−10 Hz at 1% strain (see Figures S1 and S2). Phalloidin was not added to the networks used for rheological experiments.

Confocal Imaging of Networks. Microscope chambers were constructed from KOH-cleaned microscope slides (631-1550, VWR, Germany) and coverslips (No. 1.5, 24 × 24 mm, VWR, Germany), using two strips (3 mm wide) of optically clear double-stick adhesive tape (50 μm thick, 3M, #8212). 50 μL of actin or actin-DNA sensor solution were carefully deposited in the middle of the chamber before closing it. Solutions spread when gently placing the coverslip on top. Care was taken to avoid air bubbles in the chamber. The chambers were then immediately sealed with VALAP (vaseline, lanolin, and paraffin sealant mix) and wrapped with aluminum foil to prevent photobleaching during polymerization. Imaging was performed after the completion of polymerization (1 h). Networks were imaged with a Leica TCS SP5 confocal microscope (Leica Microsystems CMS GmbH, Mannheim, Germany) to probe the morphology of the resulting networks. We recorded confocal scans across the entire depth of the networks (z-scans). A white-light laser (Koheras N94-120-02) was used for illumination at 20% maximum intensity (2.9−3.0 μW) for the sensor channel (excitation wavelength—488 nm) and 22% maximum intensity (11.0−11.5 μW) for the actin network imaging channel (excitation wavelength—647 nm). Slices (1024 × 1024 pixels) were acquired with bidirectional scans, with each line scanned 16 times (Line average = 16) at 700 Hz. The resulting field of view was 100 μm × 100 μm. A zoom factor of 2.5 was used. A pinhole size of 1 Airy unit (95.4 μm) was used, and z-stacks with 20−30 slices were obtained with a step size of 3 μm. Images were processed using the OpenCV for Python, applying Contrast Limited Adaptive Histogram Equalization (CLAHE) with a cliplimit of 5.0 and a tilegrid size of (8,8).

Fluorescence Lifetime Measurements in Aqueous Buffer and FLIM Imaging of In Vitro Actin Networks. A custom-built confocal microscope capable of fluorescence lifetime measurements was used. Excitation was performed with a linearly polarized pulsed diode laser (λ = 485 nm, pulse duration 50 ps FWHM, LDH-P-C-485B, PicoQuant) equipped with a clean-up filter (Brightline FF01-480/17, Semrock). The light of this laser was pulsed at a repetition rate of 40 MHz with a multichannel picosecond laser driver (PDL 828, "Sepia II", PicoQuant). The laser beam was coupled into a polarization-maintaining single-mode fiber (PMC-400-4.2-NA010-3-APC-250V, Schäfter and Kirchhoff GmbH). At the fiber output, the light was collimated and reflected by a dichroic mirror (FITC/TRITC Chroma Technology) into the objective lens of the microscope (UPLSAPO 60x water, 1.2 NA, Olympus). The same water-immersion objective was used to collect fluorescence from the sample. A long-pass filter (BLP01-488R-25, Semrock) was used to block back-scattered light from the laser. The emission light was focused into a pinhole of 100 μm diameter, collimated again, and refocused onto a single-photon counting avalanche photo-diode (SPCM-CD 3516 H, Excelitas Technologies GmbH & Co. KG). A multichannel picosecond event timer (HydraHarp 400, PicoQuant) recorded the detected photons from the detector with an absolute temporal resolution of 16 ps. For lifetime measurements, a droplet of 30 μL of DNA sensors, dissolved in DNA hybridization buffer (see Table S2 for buffer composition), was placed on a glass coverslip (2424 mm, thickness 170 μm). The laser beam was focused 30 μm inside the droplet, and data acquisition was started. TCSPC histograms were computed from the recorded photons and mono-exponential (opened sensors and donor-only controls) and bi-exponential (for closed sensors) decay functions were fitted to the tails of the histograms (0.5 ns after the maximum) using a maximum-likelihood procedure as described elsewhere.[41] We also performed fluorescence lifetime measurements on DNA sensors dissolved in an aqueous buffer suitable for actin networks. A further goal of *in vitro* fluorescence lifetime measurements was to search for the optimal molar ratio between the individual strands such that sufficient F strands were present for crosslinking actin filaments. It was equally important to obtain a molar ratio that ensured maximal quenching of fluorescence lifetimes. In order to meet both criteria, we varied the molar concentration of the F strand in the closed sensor and determined fluorescence lifetimes for four different molar ratios, 2:2:2, 1:2:2, 0.5:2:2, and 0.25:2:2 (F/H/Q). Table S4 and Figure S3 list the fluorescence lifetime values and TCSPC decays for all of the different constructs. These values suggest that a molar ratio of 0.5:2:2 contains sufficient F strands to meet both criteria.

For FLIM imaging on *in vitro* reconstituted actin networks, we acquired z stacks utilizing the same custom-built confocal microscope equipped with timing electronics and a three-axis piezo stage (P-562.3CD, Physical Instruments) driven with a digital piezo controller (E-710 Physical Instruments). Sensors were crosslinked into actin networks and filled into a sample chamber (as described in the Confocal Imaging of Networks section) and z stacks with a z-spacing of 1 μm were acquired until 5 μm from the coverslip surface for areas of ∼40 μm × 40 μm. TCSPC histograms were computed from collected photons corresponding to each pixel for every corresponding z slice. Fluorescence lifetimes reported in Figure 3d were obtained by fitting the mean TCSPC decay of all pixels in a slice. Results presented in Figure 3d are from a representative plane (3 μm from the surface) for closed and donor-only controls. TCSPC histograms at every z plane from 0 to 5 μm for closed and donor-only controls crosslinked to actin networks are illustrated in Figure S4. TCSPC histograms were tail-fitted using bi-exponential and mono-exponential decay functions for closed and donor-only controls, respectively (see the SI for details on fluorescence lifetime data evaluation).

RESULTS AND DISCUSSION

Our DNA force sensor consists of a hairpin with a stem (8 base pairs (bp)), a loop (16 bp), and two arms (each 20 nt) (Figure 1a). Two other strands, namely, the F and Q strands, hybridize to the hairpin arms. The FRET pair is formed by a fluorophore Alexa 488 attached to the F strand and a quencher (Iowa black FQ) attached to the Q strand (see the Experimental Section). Upon hybridization with the hairpin arms, the dye and the quencher come into the FRET range. The sensor is attached to actin through LifeAct,[42] a transient actin-binding protein (ABP) with a k_{off}^{-1} = 0.4 s in the following way. The 5′ and 3′ termini of the hairpin sensor are modified to incorporate a HaloTag ligand which binds covalently to the HaloTag protein[43] which is expressed as a genetic fusion with a red

https://doi.org/10.1021/acsanm.3c01783
ACS Appl. Nano Mater. 2023, 6, 15455−15464

fluorescent protein (RFP) and LifeAct (Figure 3a). The LifeAct construct can be used for *in cellulo* measurements via transfection of a plasmid with the three fused genes, and it can be recombinantly expressed and purified as a protein for *in vitro* measurements. When an external force acts on this sensor and exceeds a certain threshold, the sensor hairpin undergoes a conformational switch by unfolding from a closed (high FRET) to an open (low FRET) state (Figure 1a).

We first characterized our sensor using bulk fluorescence intensity measurements, in a standard fluorescence spectrometer (AMINCO-Bowman Series 2 Luminescence Spectrometer, see the Experimental Section). A "donor-only" control (Figure 1b) was used as a reference to assess the FRET efficiency of the full sensor. We designed an additional construct to force the sensor into an open state without applied force, consisting of a DNA strand complementary to the loop region of the hairpin (C strand) (orange strand in Figure 1b). In the remainder of this manuscript, we will use the following nomenclature for the various constructs: "closed sensors"—sensors in their assembled geometry having both dye and quencher molecules, "donor-only control"—assembled sensors that do not contain quencher, and "opened sensors"—sensors containing both fluorophore and quencher that are opened by the C strand. Figure 2a shows bulk fluorescence spectra of closed (red), donor-only (blue), and opened (green) sensors. The spectra confirm strong FRET-based quenching. The mean fluorescence intensity of closed sensors is 90 ± 2% quenched, compared to donor-only controls. Opened sensors (opened by C strand, green curve in Figure 2a) produce a higher fluorescence intensity than the donor-only probes (without quencher, blue curve in Figure 2a). We attribute the reduced fluorescence intensity in donor-only control probes to intra-loop quenching of the fluorophore via electron transfer by guanosine bases in close proximity.[44]

To avoid possible artifacts inherent to fluorescence intensity measurements, we measured the donor fluorescence lifetimes (τ) and used them to determine the sensor's FRET efficiency in solution. FRET efficiency is quantified using the relation

$$E = 1 - \frac{\tau_{DA}}{\tau_{D}} \quad (1)$$

where E is the FRET efficiency, and τ_{DA} and τ_{D} are the fluorescence lifetimes of the donor in the presence (closed sensor) and absence (donor-only) of the acceptor, respectively. A high FRET efficiency indicates proper assembly of the closed sensor. All fluorescence lifetime measurements were done by time-correlated single-photon counting (TCSPC) with a confocal microscope[45] (see the Experimental Section for details). Figure 2b illustrates TCSPC histograms calculated for closed sensors, donor-only controls, and opened sensors. We tail-fitted these TCSPC histograms using a suitable decay function to obtain fluorescence lifetimes (see SI section Fluorescence Lifetime Data Evaluation). Fitted fluorescence lifetime values for closed sensors were 0.5 ± 0.1 ns (46 ± 4% relative amplitude) and 3.7 ± 0.1 ns (54 ± 5% relative amplitude) indicating strong fluorescence quenching, compared to excited-state lifetime values of 3.7 ± 0.1 ns for donor-only controls from three independent measurements. Note that since we calculate FRET efficiencies using lifetimes of closed and donor-only controls only, the intra-loop quenching from guanosine is systematically taken into account. We calculate a FRET efficiency of 86.0 ± 3.2% (Figure 3e) taking into account the quenched lifetime of 0.5 ± 0.1 ns (τ_{DA}) and donor-only lifetime of 3.7 ± 0.1 ns (τ_{D}). The FRET efficiency value is in excellent agreement with the quenching efficiency observed by bulk spectroscopy. This result confirms the correct assembly of the sensors. We also observed a component with a long fluorescence lifetime for the closed sensors (3.7 ± 0.1 ns) which indicates the existence of a nonquenched subpopulation. Likely explanations are the absence of quencher strands in some of the assembled constructs or misfolding of the constructs themselves. Hence, for FRET efficiency calculations throughout this study, we only consider the lifetime of the quenched population (τ_{DA}) and exclude the nonquenched lifetimes. The measured fluorescence lifetime of opened sensors in DNA buffer was 3.9 ± 0.1 ns. This value is larger than the fluorescence lifetime of the donor-only controls, due to the quenching of fluorescence by guanosine. Additional fluorescence lifetime measurements for closed sensors containing F, H, and Q strands in various molar ratios, are also presented (Table S4). These measurements helped us to optimize sensor performance.

Next, we tested how well the functionality of sensors is preserved when they are linked to actin filaments in a network (Figure 3a,b). We checked the fluorescence intensity of closed sensors, donor-only control, and opened sensors when crosslinked into an *in vitro* reconstituted actin network (Figure 3c). We observed reduced quenching for closed sensors compared to unattached sensors in solution (Figure 2a): the fluorescence intensity of closed sensors was ∼50% of that of donor-only controls when crosslinked to actin (Figure 3c). This result implies that only ∼50% of sensors remained closed and properly assembled inside the actin network, while the remaining sensors may lack Q strands (improperly assembled) which contribute to the less strong quenching. This can be also inferred from a separate set of experiments where F and Q strands were separately attached to actin filaments, denoted as AF and AQ, respectively, and then mixed together for quenching measurements (see the SI, red curve, Figure S6). F strands attached to actin and hybridized with H strands, denoted as AF + H, showed a fluorescence intensity level similar to the that of closed sensors in actin networks (∼50% quenching) (Figure 3c). Upon addition of the AQ sample (Q strand attached to actin) to the AF+H mixture, strong quenching was observed (black curve, Figure S6). With the relatively high off-rate of LifeAct, the linker to actin, we would not expect sensors to "remember" transient forces exerted on them during mixing or while filling the chamber. Since the sensor is constructed to monitor transient forces, however, a static population of unzipped sensors does not interfere with its intended function. Control experiments in the buffer used for *in vitro* actin networks (for buffer composition, see Table S2) showed that the buffer conditions do not cause unzipping. We also optimized the stoichiometry of F, H, and Q strands in actin buffer (Table S4) to obtain maximal quenching of fluorescence emission. Sensor function was then also measured with fluorescence lifetime imaging microscopy (FLIM) (see the Experimental Section). We reconstituted two kinds of *in vitro* actin networks, one crosslinked by closed sensors and by (C strand) opened sensors, respectively, with an actin concentration of 24 μM and a molar ratio of crosslinker (sensor) to actin concentration, R = 0.1. FLIM images were recorded for areas of ∼40 μm × 40 μm from six adjacent z-planes with a spacing of 1 μm. The short (quenched)-lifetime component was found to be 0.8 ± 0.3 ns (blue bars in Figure 3d) and remained roughly constant across all z-planes.

https://doi.org/10.1021/acsanm.3c01783
ACS Appl. Nano Mater. 2023, 6, 15455−15464

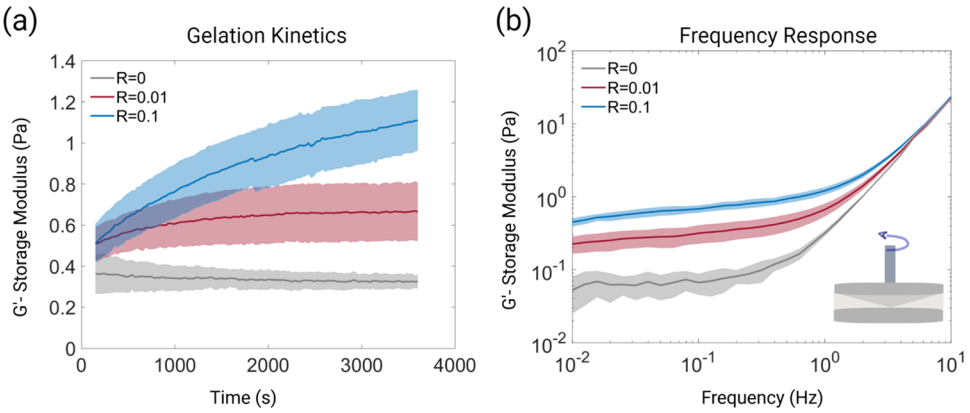

Figure 4. Rheology of actin-DNA sensor networks. (a) The effect of crosslinking of DNA sensors to actin filaments was observed via an increase in elastic shear modulus (G', blue and red curves). At a high sensor concentration ($R = 0.1$), the network became stiffer (increased G'), indicating the formation of a well-crosslinked network. (b) Frequency response of networks in the linear response range at 1% strain. Crosslinked networks exhibited weak power-law behavior in the reliably probed frequency range <1 Hz. $R = 0.01$ indicates a network with a low concentration of sensors, $R = 0.1$, is a network with a high sensor concentration, and $R = 0$ indicates an entangled actin network (no sensors). $R = c_{crosslinker}/c_{actin}$. Solid lines represent mean values and shaded areas are the standard error of the mean.

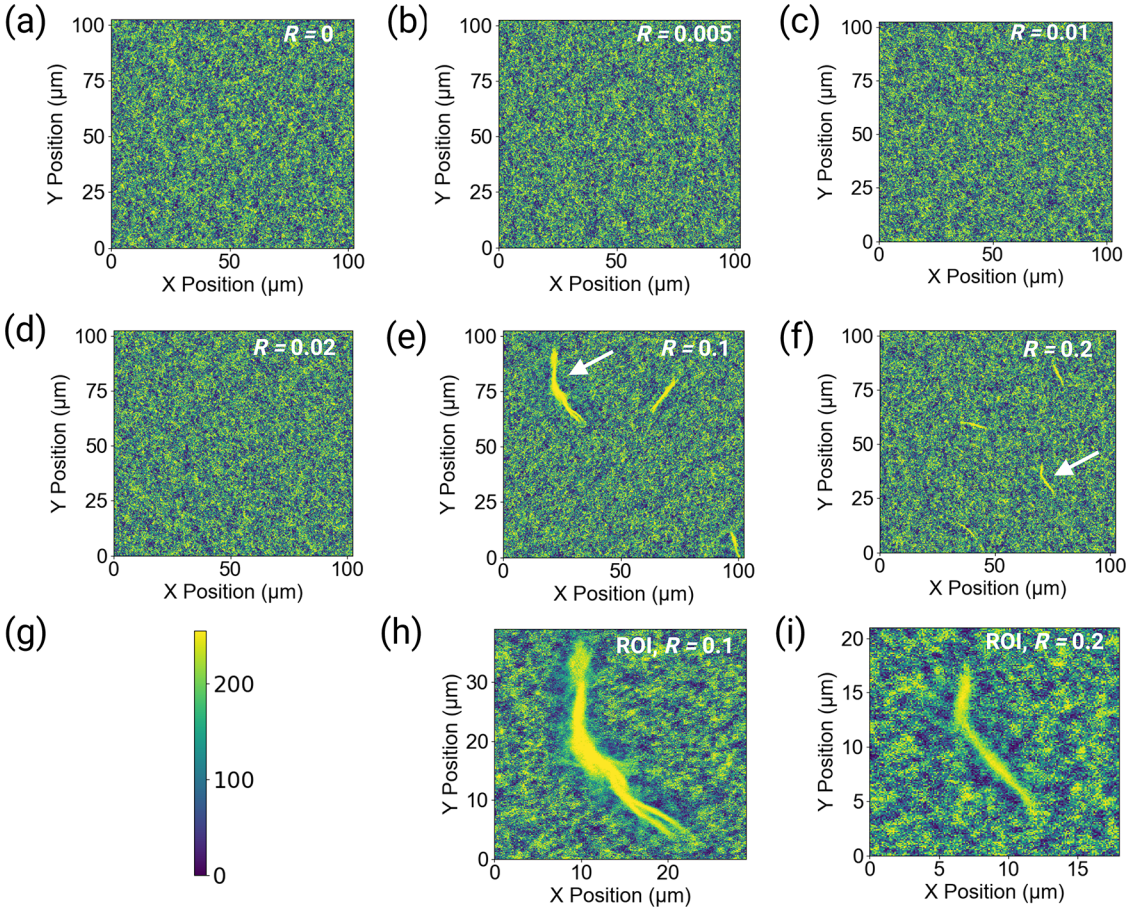

Figure 5. Morphology of DNA-sensor-crosslinked actin networks. Confocal laser scan images of (a) entangled actin ($R = 0$) and (b–f) DNA-sensor-crosslinked networks (from $R = 0.005$ to 0.2). (b–d) An isotropically crosslinked network was observed for all lower R-values ($R = 0.005$, 0.01, 0.02) which was not visibly different from an entangled actin network ($R = 0$). (e, f) At higher sensor concentrations ($R = 0.1$, 0.2), composite network structures arose, which had the appearance of bundles embedded in a crosslinked network. $R = c_{crosslinker}/c_{actin}$. (g) False-color bar displaying brightness of images. (h, i) Cropped images for ROI indicated by arrows in E and F. They show the bundling of actin filaments by the DNA sensor. Actin was fluorescently labeled with Atto 647N Phalloidin. Images were processed using contrast-limited adaptive histogram equalization.

However, we also observed a long-lifetime (nonquenched) component of 3.4 ± 0.3 ns corresponding to measurements in both types of aqueous buffers ("DNA hybridization buffer" and "Actin buffer", see Table S2) used in this study for the characterization of sensors in solution. Figure 3e shows FRET efficiencies obtained for sensors in DNA buffer only (86.1 ±

https://doi.org/10.1021/acsanm.3c01783
ACS Appl. Nano Mater. 2023, 6, 15455−15464

3.2%) and actin networks (76.9 ± 8.3%). We did observe a higher FRET efficiency in actin networks compared to quenching efficiency from bulk spectroscopy. However, in the end, high FRET efficiencies are central to ensuring the proper functionality of our sensor molecules. Hence, our designed sensor molecules are well suited for *in vitro* actin network measurements.

Crosslinking of the entangled actin networks by the sensor constructs is expected to affect the viscoelastic properties of the networks. Rheology experiments can thus help to test the efficiency of the sensor in linking different filaments as opposed to binding to the same filament. To quantitatively evaluate the viscoelastic properties of sensor-crosslinked actin networks, we measured complex shear moduli $G(\omega)$ of such networks in frequency-sweep experiments between 0.01 and 1 Hz (data unreliable above 1 Hz) at a strain amplitude of 1% in a rheometer (MCR 501, Anton Paar, see the Experimental Section). In this frequency range, we expect approximate elastic plateau (or weak power law) behavior with the real part of $G(\omega)$, the storage modulus G' (Figures 4b and S1b), being larger than the imaginary part, the viscous modulus G'' (Figure S1c). We found that, overall, sensor-crosslinked networks were substantially more rigid than entangled actin at the same concentration of 24 μM actin. Entangled actin networks showed a weak power-law response at low frequencies with a storage modulus $G' \approx 0.4$ Pa, consistent with published studies.[46−48] Sensor-crosslinked networks displayed approximate plateaus with G' ranging from 0.5 to 1.2 Pa (Figures 4a and S1a), depending on sensor concentration (given by R = crosslinker concentration (DNA sensors)/actin concentration in Table S3). At the highest sensor concentration that we tested (R = 0.2), we found G' = 1.8 Pa for 1:1:1 (F/H/Q) networks (data not shown) and G' = 1.5 Pa for 0.5:1:1 (F/H/Q) networks (Figure S1a). For high sensor concentrations (R = 0.1 and 0.2), the network elasticity increased slowly over time and had not reached a steady-state shear modulus after > 1 h (see Figure 4a for R = 0.1 and Figure S1a for R = 0.2). Networks with lower sensor concentrations (R = 0.005, 0.01, and 0.02) stabilized after ∼2000 s (Figures 4a and S1a). Both the significant increase in plateau modulus and the slow maturation of the crosslinked actin networks toward a steady state are consistent with the reported behavior of actin networks crosslinked by simple double-stranded DNA tethers without sensor functions where slow bundle formation has been seen.[49]

We did indeed observe actin bundling in sensor-crosslinked actin networks by confocal microscopy (see Experimental Section), corresponding to changes in the measured elasticity. At low sensor concentrations (R = 0.005, 0.01, 0.02), networks appeared isotropically crosslinked (Figure 5a−d). At higher sensor concentrations, R = 0.1 and 0.2 (Figure 5e,f), the networks became inhomogeneous, with denser actin bundles co-existing with a homogeneous network background. These bundles were always observed throughout the samples (Figure S2), proving that they were not surface artifacts. The slow approach to a mechanical steady state (Figure 4a, R = 0.1) observed in the rheology experiments likely reflects the ongoing formation of bundles that might eventually percolate. Bundles in our networks were observed only at high concentrations of sensors and thus could not come from phase separation driven by solvent conditions, i.e., changes in ion concentrations.[50] Bundles were also unlikely to be driven by depletion forces due to DNA. Entropy-driven bundle formation should result in a loss of connectivity/entanglements in actin.[51] This was not the case for our sensor-crosslinked actin networks since their elasticity remained high, indicating good connectivity between sensors and actin.

Finally, to establish basic feasibility, we tested the suitability of our sensors for live-cell measurements. HeLa cells were transfected with HaloTag -RFP-LifeAct, followed by microinjection of a 50 nM solution of closed DNA sensors (see Figure S7). Figures S8 and S9 show confocal micrographs of HeLa cells imaged in two spectral channels, imaging sensors and RFP-actin. The images show co-localization of sensors and actin stress fibers. By FLIM, we observed an average fluorescence lifetime of 2.2 ± 0.5 ns for the DNA sensors in the cells (Figure S8c) which is in agreement with the fluorescence lifetime values observed in *in vitro* actin networks (Figure 3d). These initial findings show that the sensors can be deployed in living cells and are likely to be applicable for intracellular force-sensing applications in the future.

CONCLUSIONS

We have constructed and tested a DNA-based molecular force sensor, designed to attach to and crosslink actin filaments either in *in vitro* reconstituted actin networks or in living cells. The sensor uses FRET between a synthetic organic dye and a quencher that can be read out using fluorescence intensity or fluorescence lifetime imaging. While we here targeted actin filaments, the sensors can, in principle, be attached to any cellular component with the help of specific binding proteins or fragments of those using the HaloTag system. We tested the sensors' optical function in reconstituted actin networks. FRET efficiencies in DNA buffer and *in vitro* sensor-crosslinked actin networks were 86.10 ± 3.2% and 76.9 ± 8.3%, respectively, which is comparable to other reported DNA force sensors that, in contrast to ours, were designed for surface attachment.[29,36] Our 8 bp hairpin DNA sensor can easily be modified by changing hairpin length and GC content to probe different force ranges.[32−36] In our case of actin crosslinking sensors, various binding tools,[52] or mutant ABPs can be employed for attachment. Binding proteins or fragments have broadly varying off-rates,[53,54] which endow the sensors with a temporal high-pass filter function: only force changes that occur faster than the inverse off-rate will be detected. This is an important feature since (i) the sensors are designed to sample changes in forces, not static forces, and (ii) the force felt by an individual sensor will depend on its binding geometry to other structural elements in the cell. In order to rapidly average over different attachment geometries before the dyes photobleach, it is advantageous to use binding motifs with reasonably high off-rates. One way to decrease off-rates, when needed, though, would be to duplicate or triplicate binding sites. The design of our sensor is a first step toward the study of force transmission across cellular biopolymer networks. A next major challenge will be to explore the effects of attachment geometry. In contrast to sensors that have been deployed between cells and substrates or were embedded in more or less 1-D load-bearing structures such as focal adhesions, the network sensors will likely bind in very inhomogeneous directions and configurations, experiencing broadly varying force on the molecular scale in deforming networks. The technology we introduced here opens the door toward sampling transient forces all-optically and noninvasively in complex 3D environments such as cells and tissues. Our first *in cellulo* trial shows that sensors can be deployed inside living cells.

https://doi.org/10.1021/acsanm.3c01783
ACS Appl. Nano Mater. 2023, 6, 15455−15464

■ ASSOCIATED CONTENT

Supporting Information

The Supporting Information is available free of charge at https://pubs.acs.org/doi/10.1021/acsanm.3c01783.

Sequences of the DNA oligos we used, buffer compositions, DNA sensor crosslinking concentrations, fluorescence lifetime values, $F_{(1/2)}$ calculations for DNA force sensor, experimental conditions used for ΔG_{fold} calculations, rheology and imaging results: gelation kinetics and frequency response of actin and actin-DNA sensor networks at various sensor concentrations, micro-structures of actin-DNA sensor networks, lifetime decay curves of sensor and donor-only probes cross-linked to actin, lifetime decay curve at each *z*-plane in the crosslinked network and decay curves of the different stoichiometry of FHQ strands in the closed sensor, schematic representation of DNA sensor transfection and microinjection protocol, and confocal micrographs of HeLa cells microinjected with DNA sensors and FLIM images of the same (PDF)

■ AUTHOR INFORMATION

Corresponding Authors

Florian Rehfeldt − *Third Institute of Physics − Biophysics, Georg August University, 37077 Göttingen, Germany; Experimental Physics I, University of Bayreuth, 95440 Bayreuth, Germany;* orcid.org/0000-0001-9086-3835; Email: florian.rehfeldt@uni-bayreuth.de

Christoph F. Schmidt − *Third Institute of Physics − Biophysics, Georg August University, 37077 Göttingen, Germany; Department of Physics and Soft Matter Center, Duke University, Durham, North Carolina 27708, United States;* orcid.org/0000-0003-2864-6973; Email: cfschmidt@phy.duke.edu

Authors

Christina Jayachandran − *Third Institute of Physics − Biophysics, Georg August University, 37077 Göttingen, Germany; Department of Pharmacy - Center for Drug Research, Pharmaceutical Biology, Ludwig-Maximilians University, Munich, Bavaria 81377, Germany*

Arindam Ghosh − *Third Institute of Physics − Biophysics, Georg August University, 37077 Göttingen, Germany; Department of Biotechnology and Biophysics, Biocenter, University of Würzburg, Am Hubland 97074 Würzburg, Germany;* orcid.org/0000-0002-5712-1271

Meenakshi Prabhune − *Third Institute of Physics − Biophysics, Georg August University, 37077 Göttingen, Germany;* Present Address: Synthego, 3565 Haven Ave, Menlo Park, California 94025, United States

Jonathan Bath − *Department of Physics, Clarendon Laboratory, University of Oxford, Oxford OX1 3PU, U.K.; The Kavli Institute for Nanoscience Discovery, University of Oxford, Oxford OX1 3QU, U.K.*

Andrew J. Turberfield − *Department of Physics, Clarendon Laboratory, University of Oxford, Oxford OX1 3PU, U.K.; The Kavli Institute for Nanoscience Discovery, University of Oxford, Oxford OX1 3QU, U.K.;* orcid.org/0000-0002-3876-0190

Lara Hauke − *Third Institute of Physics − Biophysics, Georg August University, 37077 Göttingen, Germany; Institute of Pharmacology and Toxicology, University Medical Center, 37075 Göttingen, Germany;* orcid.org/0000-0003-0777-6859

Jörg Enderlein − *Third Institute of Physics − Biophysics, Georg August University, 37077 Göttingen, Germany; Cluster of Excellence "Multiscale Bioimaging: from Molecular Machines to Networks of Excitable Cells" (MBExC), Universitätsmedizin Göttingen, 37075 Göttingen, Germany;* orcid.org/0000-0001-5091-7157

Complete contact information is available at: https://pubs.acs.org/10.1021/acsanm.3c01783

Author Contributions

¶C.J. and A.G. contributed equally to this work. F.R. and C.F.S. conceived the study. F.R., C.F.S., A.T., and M.P. designed the DNA constructs. M.P. performed preliminary experiments. C.J. contributed to sensor preparation, bulk fluorescence, network imaging, rheology, and cell culture. A.G. performed the FLIM experiments reported here. L.H. performed microinjection experiment in cells. J.E. supervised the FLIM experiments. F.R. and C.F.S. supervised all other experiments., C.J., A.G., J.E., F.R., and C.F.S. wrote the manuscript.

Notes

The authors declare no competing financial interest.

■ ACKNOWLEDGMENTS

The authors thank Fred Wouters for insightful discussions and the lab of Khalid Salaita for their input on FLIM measurements. This work was financially supported by the Deutsche Forschungsgemeinschaft (DFG, German Research Foundation) via project A03 (M.P., C.J., F.R., and C.F.S.) of the Collaborative Research Center 755 (SFB 755). A.G. and J.E. thank financial support by the Deutsche Forschungsgemeinschaft (DFG) through project A06 of the SFB 860. J.E. is grateful for financial support by the Deutsche Forschungsgemeinschaft (DFG, German Research Foundation) under Germany's Excellence Strategy-EXC 2067/1-390729940. Figures 1, and 3 were prepared with Biorender.

■ REFERENCES

(1) Hayakawa, K.; Tatsumi, H.; Sokabe, M. Actin filaments function as a tension sensor by tension-dependent binding of cofilin to the filament. *J. Cell Biol.* **2011**, *195*, 721−727.

(2) Hotulainen, P.; Lappalainen, P. Stress fibers are generated by two distinct actin assembly mechanisms in motile cells. *J. Cell Biol.* **2006**, *173*, 383−394.

(3) Dasanayake, N. L.; Michalski, P. J.; Carlsson, A. E. General mechanism of actomyosin contractility. *Phys. Rev. Lett.* **2011**, *107*, No. 118101.

(4) Soares e Silva, M.; Depken, M.; Stuhrmann, B.; Korsten, M.; MacKintosh, F. C.; Koenderink, G. H. Active multistage coarsening of actin networks driven by myosin motors. *Proc. Nat. Acad. Sci. U.S.A.* **2011**, *108*, 9408−9413.

(5) Scholey, J. M.; Brust-Mascher, I.; Mogilner, A. Cell division. *Nature* **2003**, *422*, 746−752.

(6) McBeath, R.; Pirone, D. M.; Nelson, C. M.; Bhadriraju, K.; Chen, C. S. Cell shape, cytoskeletal tension, and RhoA regulate stem cell lineage commitment. *Dev. Cell* **2004**, *6*, 483−495.

(7) Cojoc, D.; Difato, F.; Ferrari, E.; Shahapure, R. B.; Laishram, J.; Righi, M.; Di Fabrizio, E. M.; Torre, V. Properties of the force exerted by filopodia and lamellipodia and the involvement of cytoskeletal components. *PLoS One* **2007**, *2*, No. e1072.

(8) Ridley, A. J.; Schwartz, M. A.; Burridge, K.; Firtel, R. A.; Ginsberg, M. H.; Borisy, G.; Parsons, J. T.; Horwitz, A. R. Cell

migration: integrating signals from front to back. *Science* **2003**, *302*, 1704−1709.
(9) Welch, M. D.; Mullins, R. D. Cellular control of actin nucleation. *Annu. Rev. Cell Dev. Biol.* **2002**, *18*, 247−288.
(10) Pollard, T. D.; Borisy, G. G. Cellular motility driven by assembly and disassembly of actin filaments. *Cell* **2003**, *112*, 453−465.
(11) Engler, A. J.; Sen, S.; Sweeney, H. L.; Discher, D. E. Matrix elasticity directs stem cell lineage specification. *Cell* **2006**, *126*, 677−689.
(12) Zemel, A.; Rehfeldt, F.; Brown, A.; Discher, D.; Safran, S. Optimal matrix rigidity for stress-fibre polarization in stem cells. *Nat. Phys.* **2010**, *6*, 468−473.
(13) Rehfeldt, F.; Engler, A. J.; Eckhardt, A.; Ahmed, F.; Discher, D. E. Cell responses to the mechanochemical microenvironment−implications for regenerative medicine and drug delivery. *Adv. Drug Delivery Rev.* **2007**, *59*, 1329−1339.
(14) Kaliman, S.; Jayachandran, C.; Rehfeldt, F.; Smith, A.-S. Novel growth regime of MDCK II model tissues on soft substrates. *Biophys. J.* **2014**, *106*, L25−L28.
(15) Geiger, B.; Spatz, J. P.; Bershadsky, A. D. Environmental sensing through focal adhesions. *Nat. Rev. Mol. Cell Biol.* **2009**, *10*, 21−33.
(16) Polacheck, W. J.; Chen, C. S. Measuring cell-generated forces: a guide to the available tools. *Nat. Methods* **2016**, *13*, 415−423.
(17) Rief, M.; Gautel, M.; Oesterhelt, F.; Fernandez, J. M.; Gaub, H. E. Reversible unfolding of individual titin immunoglobulin domains by AFM. *Science* **1997**, *276*, 1109−1112.
(18) Fisher, T. E.; Oberhauser, A. F.; Carrion-Vazquez, M.; Marszalek, P. E.; Fernandez, J. M. The study of protein mechanics with the atomic force microscope. *Trends Biochem. Sci.* **1999**, *24*, 379−384.
(19) Ashkin, A.; Dziedzic, J. M. Optical trapping and manipulation of viruses and bacteria. *Science* **1987**, *235*, 1517−1520.
(20) Schlosser, F.; Rehfeldt, F.; Schmidt, C. F. Force fluctuations in three-dimensional suspended fibroblasts. *Philos. Trans. R. Soc. Lond., B, Biol. Sci.* **2015**, *370*, No. 20140028.
(21) Smith, S. B.; Finzi, L.; Bustamante, C. Direct mechanical measurements of the elasticity of single DNA molecules by using magnetic beads. *Science* **1992**, *258*, 1122−1126.
(22) Förster, T. Zwischenmolekulare Energiewanderung und Fluoreszenz. *Ann. Phys.* **1948**, *437*, 55−75.
(23) Liu, Y.; Galior, K.; Ma, V. P.-Y.; Salaita, K. Molecular tension probes for imaging forces at the cell surface. *Acc. Chem. Res.* **2017**, *50*, 2915−2924.
(24) Meng, F.; Suchyna, T. M.; Sachs, F. A fluorescence energy transfer-based mechanical stress sensor for specific proteins in situ. *FEBS J.* **2008**, *275*, 3072−3087.
(25) Grashoff, C.; Hoffman, B. D.; Brenner, M. D.; Zhou, R.; Parsons, M.; Yang, M. T.; McLean, M. A.; Sligar, S. G.; Chen, C. S.; Ha, T.; Schwartz, M. A. Measuring mechanical tension across vinculin reveals regulation of focal adhesion dynamics. *Nature* **2010**, *466*, 263−266.
(26) Stabley, D. R.; Jurchenko, C.; Marshall, S. S.; Salaita, K. S. Visualizing mechanical tension across membrane receptors with a fluorescent sensor. *Nat. Methods* **2012**, *9*, 64−67.
(27) Jurchenko, C.; Chang, Y.; Narui, Y.; Zhang, Y.; Salaita, K. S. Integrin-generated forces lead to streptavidin-biotin unbinding in cellular adhesions. *Biophys. J.* **2014**, *106*, 1436−1446.
(28) Wang, X.; Ha, T. Defining single molecular forces required to activate integrin and notch signaling. *Science* **2013**, *340*, 991−994.
(29) Shroff, H.; Reinhard, B. M.; Siu, M.; Agarwal, H.; Spakowitz, A.; Liphardt, J. Biocompatible force sensor with optical readout and dimensions of 6 nm3. *Nano Lett.* **2005**, *5*, 1509−1514.
(30) Dutta, P. K.; Zhang, Y.; Blanchard, A. T.; Ge, C.; Rushdi, M.; Weiss, K.; Zhu, C.; Ke, Y.; Salaita, K. Programmable multivalent DNA-origami tension probes for reporting cellular traction forces. *Nano Lett.* **2018**, *18*, 4803−4811.
(31) Sarkar, A.; LeVine, D.; Zhao, Y.; Mollaeian, K.; Ren, J.; Wang, X. Tandem Tension Sensor Reveals Substrate Rigidity-Dependence of Integrin Molecular Tensions in Live Cells. *bioRxiv* **2020**, DOI: 10.1101/2020.01.24.918946.
(32) Prabhune, M.; Rehfeldt, F.; Schmidt, C. F. Molecular force sensors to measure stress in cells. *J. Phys. D: Appl. Phys.* **2017**, *50*, No. 233001.
(33) Liphardt, J.; Onoa, B.; Smith, S. B.; Tinoco, I.; Bustamante, C. Reversible unfolding of single RNA molecules by mechanical force. *Science* **2001**, *292*, 733−737.
(34) Woodside, M. T.; Anthony, P. C.; Behnke-Parks, W. M.; Larizadeh, K.; Herschlag, D.; Block, S. M. Direct measurement of the full, sequence-dependent folding landscape of a nucleic acid. *Science* **2006**, *314*, 1001−1004.
(35) Woodside, M. T.; Behnke-Parks, W. M.; Larizadeh, K.; Travers, K.; Herschlag, D.; Block, S. M. Nanomechanical measurements of the sequence-dependent folding landscapes of single nucleic acid hairpins. *Proc. Nat. Acad. Sci. U.S.A.* **2006**, *103*, 6190−6195.
(36) Zhang, Y.; Ge, C.; Zhu, C.; Salaita, K. DNA-based digital tension probes reveal integrin forces during early cell adhesion. *Nat. Commun.* **2014**, *5*, No. 5167.
(37) Zadeh, J. N.; Steenberg, C. D.; Bois, J. S.; Wolfe, B. R.; Pierce, M. B.; Khan, A. R.; Dirks, R. M.; Pierce, N. A. NUPACK: analysis and design of nucleic acid systems. *J. Comput. Chem.* **2011**, *32*, 170−173.
(38) Frederiksen, D. W.; Cunningham, L. W. *Structural and Contractile Proteins: Part B*; Academic Press, 1982.
(39) Pardee, J. D.; Spudich, J. A. [18] Purification of muscle actin. *Methods Enzymol.* **1982**, *85*, 164−181.
(40) MacLean-Fletcher, S.; Pollard, T. D. Identification of a factor in conventional muscle actin preparations which inhibits actin filament self-association. *Biochem. Biophys. Res. Commun.* **1980**, *96*, 18−27.
(41) Ghosh, A.; Sharma, A.; Chizhik, A. I.; Isbaner, S.; Ruhlandt, D.; Tsukanov, R.; Gregor, I.; Karedla, N.; Enderlein, J. Graphene-based metal-induced energy transfer for sub-nanometre optical localization. *Nat. Photonics* **2019**, *13*, 860−865.
(42) Riedl, J.; Crevenna, A. H.; Kessenbrock, K.; Yu, J. H.; Neukirchen, D.; Bista, M.; Bradke, F.; Jenne, D.; Holak, T. A.; Werb, Z.; et al. Lifeact: a versatile marker to visualize F-actin. *Nat. Methods* **2008**, *5*, 605−607.
(43) Los, G. V.; Encell, L. P.; McDougall, M. G.; Hartzell, D. D.; Karassina, N.; Zimprich, C.; Wood, M. G.; Learish, R.; Ohana, R. F.; Urh, M.; et al. HaloTag: a novel protein labeling technology for cell imaging and protein analysis. *ACS Chem. Biol.* **2008**, *3*, 373−382.
(44) Noble, J. E.; Wang, L.; Cole, K. D.; Gaigalas, A. K. The effect of overhanging nucleotides on fluorescence properties of hybridising oligonucleotides labelled with Alexa-488 and FAM fluorophores. *Biophys. Chem.* **2005**, *113*, 255−263.
(45) Benda, A.; Hof, M.; Wahl, M.; Patting, M.; Erdmann, R.; Kapusta, P. TCSPC upgrade of a confocal FCS microscope. *Rev. Sci. Instrum.* **2005**, *76*, No. 033106.
(46) Koenderink, G. H.; Atakhorrami, M.; MacKintosh, F.; Schmidt, C. F. High-frequency stress relaxation in semiflexible polymer solutions and networks. *Phys. Rev. Lett.* **2006**, *96*, No. 138307.
(47) Gittes, F.; Schnurr, B.; Olmsted, P.; MacKintosh, F. C.; Schmidt, C. F. Microscopic viscoelasticity: shear moduli of soft materials determined from thermal fluctuations. *Phys. Rev. Lett.* **1997**, *79*, 3286.
(48) Atakhorrami, M.; Sulkowska, J. I.; Addas, K.; Koenderink, G.; Tang, J.; Levine, A.; MacKintosh, F.; Schmidt, C. Correlated fluctuations of microparticles in viscoelastic solutions: Quantitative measurement of material properties by microrheology in the presence of optical traps. *Phys. Rev. E* **2006**, *73*, No. 061501.
(49) Lorenz, J. S.; Schnauß, J.; Glaser, M.; Sajfutdinow, M.; Schuldt, C.; Käs, J. A.; Smith, D. M. Synthetic Transient Crosslinks Program the Mechanics of Soft, Biopolymer-Based Materials. *Adv. Mater.* **2018**, *30*, No. 1706092.
(50) Zribi, O. V.; Kyung, H.; Golestanian, R.; Liverpool, T. B.; Wong, G. C. Condensation of DNA-actin polyelectrolyte mixtures

driven by ions of different valences. *Phys. Rev. E* **2006**, *73*, No. 031911.
(51) Fitzpatrick, R.; Michieletto, D.; Peddireddy, K. R.; Hauer, C.; Kyrillos, C.; Gurmessa, B. J.; Robertson-Anderson, R. M. Synergistic interactions between DNA and actin trigger emergent viscoelastic behavior. *Phys. Rev. Lett.* **2018**, *121*, No. 257801.
(52) Melak, M.; Plessner, M.; Grosse, R. Actin visualization at a glance. *J. Cell Sci.* **2017**, *130*, 525−530.
(53) Ward, S. M. V.; Weins, A.; Pollak, M. R.; Weitz, D. A. Dynamic viscoelasticity of actin cross-linked with wild-type and disease-causing mutant α-actinin-4. *Biophys. J.* **2008**, *95*, 4915−4923.
(54) Weins, A.; Schlondorff, J. S.; Nakamura, F.; Denker, B. M.; Hartwig, J. H.; Stossel, T. P.; Pollak, M. R. Disease-associated mutant α-actinin-4 reveals a mechanism for regulating its F-actin-binding affinity. *Proc. Nat. Acad. Sci. U.S.A.* **2007**, *104*, 16080−16085.

https://doi.org/10.1021/acsanm.3c01783
ACS Appl. Nano Mater. 2023, 6, 15455−15464